Differential analysis of biomolecular rupture forces

2006 J. Phys.: Condens. Matter 18 S581

(http://iopscience.iop.org/0953-8984/18/18/S06)

INSTITUTE OF PHYSICS PUBLISHING JOURNAL OF PHYSICS: CONDENSED MATTER

J. Phys.: Condens. Matter **18** (2006) S581–S599 doi:10.1088/0953-8984/18/18/S06

Differential analysis of biomolecular rupture forces

Christian H Albrecht[1], **Hauke Clausen-Schaumann**[2] **and Hermann E Gaub**[1,3]

[1] Chair of Applied Physics, LMU-München, Amalienstrasse 54, D-80799 Munich, Germany
[2] Munich University for Applied Sciences, Lothstrasse 34, D-80335 Munich, Germany

E-mail: gaub@physik.uni-muenchen.de

Received 20 September 2005
Published 19 April 2006
Online at stacks.iop.org/JPhysCM/18/S581

Abstract

After a brief overview over the development of single molecule force spectroscopy and the basic concepts of bond dissociation under external force, we discuss the recently developed differential force assay, where a molecular bond serves as a microscopic force sensor. We introduce the basic concept of this novel biomolecular assay, discuss its requirements, capabilities and limitations, and present the latest advances in the design of the assay itself, as well as its appropriate hardware. The necessary data analysis procedures are introduced, and recent results showing the discrimination of single CC and GG mismatches within a 30 base pair DNA duplex are presented.

1. Introduction

The mechanical properties of biomolecules are closely related to their molecular structure and they are key parameters in understanding their biological function [1]. Consequently, techniques which allow the precise application and measurement of piconewton forces have provided new insights into the mechanisms governing biological phenomena at the molecular level. Today, in addition to material science, physical and physical chemistry aspects, research areas in force spectroscopy cover a broad range of biologically relevant topics, like molecular motors, protein folding, nucleic acid base pairing, or enzyme–substrate and receptor–ligand binding [2–5]. Moreover, especially intermolecular forces, like the ones involved in receptor–ligand binding and nucleic acid base pairing, also play a key role in a number of technological applications: from the detection of pathogens to the quantification of messenger RNA and proteins, the vast majority of assays in biomedical diagnostics rely on receptor–ligand binding or nucleic acid base pairing, with DNA and protein biochips being only two prominent examples. Furthermore, a large number of drugs and toxins interfere with protein–substrate binding or nucleic acid base pairing in one way or another.

[3] Author to whom any correspondence should be addressed.

Unlike the more traditional methods of studying receptor–ligand binding and nucleic acid base pairing, such as micro-calorimetry, UV-absorption spectroscopy, or mass and refractive index sensitive techniques, like the quartz crystal microbalance or surface plasmon resonance spectroscopy, the dissociation of the molecular bonds by mechanical force allows not only for the quantification of binding enthalpies and reaction rate constants, but it can also provide detailed insights into binding potential landscapes and into the binding mechanisms.

1.1. Tools for measuring intermolecular forces

With the introduction of the surface force apparatus (SFA) by Tabor and Israelachvili, more than 30 years ago, the precise quantification of intermolecular and surface forces became possible for the first time [6]. In the SFA, two crossed cylindrical mica sheets are brought into close proximity with each other. The distance between the two sheets is determined by reflection interference contrast microscopy (RICM) and controlled by lever arms, while the force acting between the two sheets is measured with a mechanical spring. If the mica sheets are brought into contact, the contact area is usually of the order of several square microns, and the contact is established from the centre of the contact area towards the rim [7].

Electrostatic double layer forces, hydration and van der Waals forces, steric repulsion, friction and the forces governing molecular recognition have been studied with the surface force apparatus [8–10]. However, in the SFA, the contact area is still large, compared to molecular dimensions, and thus the intermolecular forces of many molecules act in concert. Because force is a directional parameter and binding forces in biological and chemical bonds depend on the direction of the applied force, as well as the distance along the reaction coordinate, it is not sufficient to just divide the measured force by the number of bonds probed. Therefore, in order to assess binding forces and binding potential landscapes of such bonds, a large number of molecules must be synchronized in time and space, and the number of bonds rupturing simultaneously must be precisely known. Although, with the SFA, this may in principle be accomplished, an alternative approach has been developed over the past 15 years: in single molecule force spectroscopy, one individual molecule is probed at a time and a synchronization of molecules is no longer necessary. This simplifies the experimental protocol considerably, and it makes the interpretation of the data straightforward, as incomplete synchronization and variable numbers of rupturing bonds cannot obscure the results. The most prominent techniques in single molecule force spectroscopy include optical and magnetic tweezers, glass micro-needles, the bio-membrane force probe (BFP), and most dominantly the atomic force microscopy (AFM)-based methods [7, 2]. In a typical experiment, a single molecule or molecular complex is anchored between a microscopic force sensor and an actuator which can be positioned with ångström precision. As the actuator is shortened, strain is built up within the molecule or between the partners of the molecular complex and the force sensor is displaced, by a small amount. Usually, for small displacements, the sensor displacement is proportional to the exerted force and can be detected for example by optical methods. In the case of the AFM, for example, the molecular complex is attached at one side to the substrate surface and at the other side to the sharp tip at the end of the cantilever spring. As the substrate or the cantilever is displaced by the piezo actuators, strain is built up, and the cantilever is deflected. The deflection of the cantilever is then detected via an optical lever and a position sensitive photodiode (cf also figure 1) [11].

1.2. The bond-rupture processes—thermally activated bond rupture versus quasi-static dissociation

In general, two different situations have to be considered, when molecular bonds, such as receptor–ligand bonds or nucleic acid base pairs, are ruptured apart by an external force. In

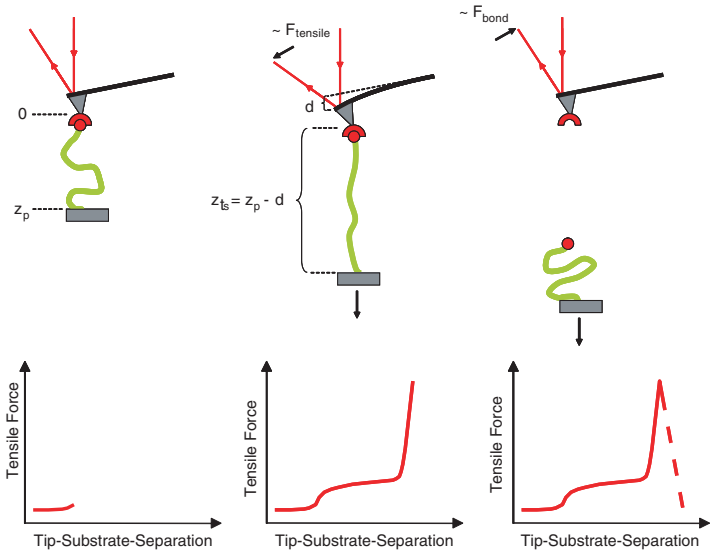

Figure 1. *AFM*. Schematic set-up of an AFM-based force spectroscopy experiment (top) and of the corresponding force trace (bottom) of a single-molecular bond attached to a polymer tether (a). Stretching of the polymer tether reveals details of the polymer elasticity: a tensile force F_{tensile} is exerted via the polymer and molecular bond to the AFM cantilever. The cantilever is displaced by a distance d, which is proportional to the exerted force, and the displacement is detected with an optical lever (b). When the tensile strength of the bond is exceeded, the molecular bond ruptures and the cantilever snaps back to its equilibrium position. The relaxation of the cantilever is proportional to the bond-rupture force F_{bond} (c). Reprinted with permission from [11]. Copyright, 2005, American Chemical Society, Washington, DC.

most cases, the binding partners are quickly separated from each other upon rupturing of the bond, so that the on-reaction is no longer possible. In this case, the on-rate is practically slowed down to zero. The bond rupture is irreversible and the whole rupture process occurs far from thermodynamic equilibrium. At the same time, the off-rate increases with increasing force, because the force effectively lowers the height of the energy barrier which must be overcome for spontaneous bond dissociation. According to a simple linear model proposed by Zhurkov and Bell [12, 13], and then elaborated by Evans *et al* [14–16], the energy barrier ΔG^* in the Arrhenius-rate function of the off-reaction is reduced by $f x_\beta$, where f is the applied force and x_β denotes the separation of the potential minimum and the dissociation barrier. The force dependent off-rate $k_{\text{off}}(f)$ then becomes

$$k_{\text{off}}(f) = \nu \exp\left(-\frac{\Delta G^* - f x_\beta}{k_B T}\right), \tag{1}$$

where ν is the force independent frequency factor, which depends on the curvature of the binding potential at its minimum, $\Delta G^* - f x_\beta$ is the effective height of the dissociation energy barrier under force, k_B is the Boltzmann constant, and T the temperature. Because $1/\nu$ is usually much smaller than the typical timescale of a force experiment, the dissociation barrier is probed many times during the experiment. Consequently, the bond dissociation under force is a thermally activated process and the observed rupture force depends on the timescale of the experiment. Fast loading of the bond will lead to a higher bond rupture force than slow loading, because shorter bond lifetimes require higher forces, as can be seen from equation (1). Using $k_{\text{off}}(f)$ from equation (1), bond rupture probability distributions and unbinding forces can be

derived in a straightforward manner [14, 16]. For a constant force loading rate $\mathrm{d}f/\mathrm{d}t$ the most probable bond rupture force f^*—i.e. the maximum of the rupture probability distribution—depends logarithmically on the force loading rate, as long as the binding potential has a single dissociation barrier. In a semilogarithmic representation of bond rupture force versus the logarithm of the force loading rate, the width of the potential, as given by x_b, can be derived from the slope of the graph, and its intersect with the $\ln(\mathrm{d}f/\mathrm{d}t)$ axis gives the off-rate at zero force. For multi-barrier potentials, the semilogarithmic representation of f^* and $\mathrm{d}f/\mathrm{d}t$ exhibits several distinct regions with different slopes, each representing the distance to the next internal separation barrier [17].

On the other hand, if a large number of consecutive bonds has to rupture in series, before the binding partners are effectively separated, both off-reaction and on-reaction can occur during the time course of the experiment. As long as the reaction rates are fast, compared to the experimental timescale, the rupture process is a fully reversible equilibrium process. In such a case the observed rupture force does not depend on the timescale of the experiment and therefore is independent of the force loading rate. A prominent example is the unzipping of long DNA duplexes which are attached to soft springs. Here on-rates and off-rates are of the order of several kilo-base-pairs per second, which is fast compared to a typical force experiment [18–22].

1.3. New tools for measuring intermolecular forces—small force sensors and symmetric designs

Today, with state of the art instrumentation, within a given bandwidth, the force resolution, i.e. the smallest detectable force f_min, is limited only by Brownian motion of the force sensor, which, according to the fluctuation-dissipation theorem, depends on temperature and on the viscous damping of the sensor:

$$f_\mathrm{min} = \sqrt{4k_\mathrm{B}TRB}, \tag{2}$$

where k_B is the Boltzmann constant, T is the temperature, R is the coefficient of viscous damping and B is the bandwidth [23, 24]. Smaller sensors experience less viscous damping, and within the desired bandwidth, the smallest detectable force f_min is therefore a function of temperature and of the size of the sensor. In recent years, several attempts have been made to reduce the size of the cantilever spring in AFM-based set-ups. Viani *et al* have demonstrated that the thermal noise of an AFM cantilever can be reduced by a factor of five, if the size of the cantilever is reduced by one order of magnitude [24]. However, as the size of the cantilever is reduced, it is crucial that the lever maintains a spring constant of the order of a few millinewtons per metre (mN m^{-1}), because otherwise detector and other instrumental noise sources may start to play a role and the assumption that the force resolution is only limited by Brownian motion of the cantilever no longer holds true. As further miniaturization of AFM cantilevers remains technologically challenging, alternative routes have to be explored, to further improve the force resolution. With bead-based techniques, like optical and magnetic tweezers, the miniaturization of the sensors, i.e. the trapped beads, seems somewhat simpler; however, here miniaturization goes at the expense of the accessible force range, as with small beads only small forces may be exerted, while receptor–ligand bond rupture forces can be of the order of a few hundred piconewtons (pN).

A conceptually different and very simple approach to reduce the size of the force sensor to a few nanometres is the use of a single molecular bond as a force standard, to which the sample bond is directly compared. In this case, the sample bond must be linked to the force standard, also referred to as the reference bond, and the external force must be applied to the sample

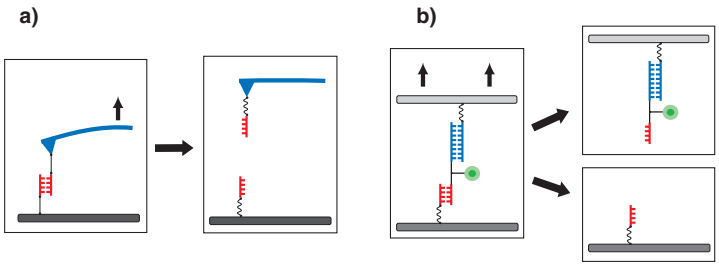

Figure 2. *AFM and DFA*. Comparison of rupture force measurements by atomic force microscopy (a) and differential force assay (b). Upon separation of the two surfaces the polymeric anchors are stretched and the force acting along the molecular complex is slowly built up. The weaker of the two molecular bonds will rupture first and as a result the label will end up on either side.

and the reference bond in series. One experimental realization of such a set-up is depicted in figure 2. Figure 2(a) shows a typical AFM set-up, where a DNA duplex is attached to an AFM tip and the substrate surface. Here the tensile force which is needed to rupture the DNA duplex is detected via the AFM cantilever spring. Figure 2(b) shows a set-up where a molecular complex consisting of a sample bond (red) and a reference DNA duplex (blue) is connected to two adjacent surfaces via polymeric anchors. As the two surfaces are separated, the force acting on the bonds in series gradually builds up until eventually the weaker bond fails. A fluorescent label, which is positioned between the two possible rupture sites, is used to identify which one of the two molecular bonds actually has ruptured. This approach has been introduced in a recent paper by Albrecht *et al* [25], where single base mutations in DNA have been detected based on bond rupture forces. A similar set-up, where the external force is applied and also monitored through an optical trap and again fluorescence is used to determine which bond ruptures, has recently been described by Lang *et al* [26].

In addition to reducing the size of the sensor, the scheme described here also increases the symmetry in single molecule force experiments. In conventional set-ups, intermolecular forces are determined via the deformation or deflection of micrometre sized springs, while here, intermolecular forces are directly compared to each other in a differential measurement format. This is analogous to weighing macroscopic objects with either scales or mechanical springs, where it is immediately evident that even with a crude scale balance small weight differences can be accurately detected, because the same physical parameters are directly compared, whereas, when a spring is used, a much more sophisticated device is required. In fact, it is a fundamental principle that small differences or small changes in a physical parameter can be most accurately determined if the difference is directly measured.

Furthermore, as has been discussed above, the forced separation of molecular bonds is a thermally activated, statistical process. Therefore a large number of rupture experiments must be carried out for each type of molecular bond. With a set-up like the one depicted in figure 2(b), it is possible to probe many molecules at the same time, because large numbers of molecules can be easily assembled between the two surfaces and probed simultaneously. Here it is important to note that the intermolecular forces are still characterized on the single molecule level, as each sample bond is individually probed by its own reference bond. Neither the macroscopic forces acting between the two surfaces nor their separation need to be determined, and the synchronization and quantification of molecules can therefore be avoided. Finally, this set-up is also capable of multiplexing, as it is compatible with chip-based assay formats, as are widely used in bio-analytics and biomedical diagnostics [27–29]. For this purpose different molecular complexes may be assembled in different spots on the substrate surface and then be connected

to the second (top) surface. Instead of measuring equilibrium binding constants, as is done with conventional biochips, the mechanical strength of the molecular bonds that have formed on the chip can be measured. This has several potential advantages over conventional chip-based assays. Assay times can be reduced, because thermodynamic equilibrium is not required, and low off-rates and rebinding do not require time-consuming washing steps. By selecting appropriate reference molecules, stringent assay conditions can be achieved locally for all spots on a chip, even if the different analyte molecules have different binding constants. And finally, in multiplexed sandwich immuno-assays, the specificity of the assay can be drastically increased, because two chip surfaces, rather than one, can be used for antigen specific encoding, as has been shown by Blank *et al* [30].

Here we give an overview over the present state of the development of the differential force assay, its capabilities and limitations. We describe recent advances, which include a motor and piezo controlled contact device, combined with a reflection interference contrast microscope for accurate distance and velocity control, an improved design of the micro-structured surfaces and surface chemistry, and we compare the assay and assay results to data obtained by other methods well as to theoretical modelling.

2. Methods

2.1. A detailed description of the differential force assay

Let us now take a more detailed look at the differential force assay and its requirements, capabilities and limitations. For convenience the differential force assay will be abbreviated as DFA in the following parts of this paper. For the complex containing the sample and reference bonds, as well as the fluorescence label, the term differential rupture complex or DRC will be used. Similar to the field of biochip technologies, the disposables of the DFA consist of chip surfaces containing immobilized biomolecules, and a fluorescence scanner serves as the readout instrument. However, in addition to more conventional biochip formats, a device for contacting and pulling apart the two chip surfaces is required. Like other chip formats, the DFA allows for the parallel measurement of multiple samples at once. In its present state 16 sample spots are deposited on an area of 1 cm $\times$ 1 cm, in a 4 $\times$ 4 array. Nevertheless, further parallelization through miniaturization is possible with more sophisticated micro-spotting devices.

A typical DFA experiment is depicted in figure 3. The assembly of the DRC starts with the covalent immobilization of the amino-modified DNA-oligomer (oligo) onto the bottom surface (the glass slide). The fluorescently labelled oligo is then hybridized to the amino-modified oligo. In the next step a biotin-labelled oligo is hybridized to the fluorescently labelled oligo, thereby completing the *DRC*. This initial situation is depicted in figure 3 on the left-hand side. Now, the upper chip surface (the silicone stamp), which is coated with a streptavidin layer is lowered, until the biotin-labelled oligo can bind to the streptavidin by molecular recognition and form a high affinity bond (middle). As the silicone stamp is withdrawn again from the glass slide, a loading force gradually builds up within the DRCs, until one of the two DNA duplexes within each DRC ruptures (right-hand side). As a result, the fluorescence label within each DRC ends up alongside the intact bond. The fluorescence intensities on both the silicone stamp and the glass slide are then determined using a fluorescence scanner. Note that during the chip separation, each DRC is loaded and probed individually so that the overall force acting between the chip surfaces does not affect the outcome of the assay.

This differential force measurement is a unique feature of the DFA, which also shares a number of features with other methods like AFM, SFA, as well as micro-contact printing (μCP), as will be pointed out in the following sections.

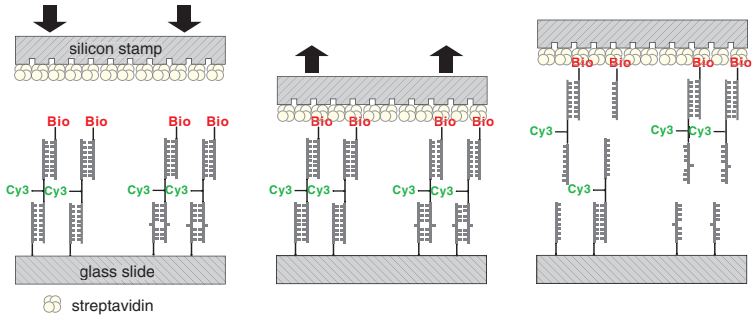

Figure 3. *DFA process.* Schematic diagrams of the differential force assay with oligo nucleotides. Two spots each containing two identical molecular rupture complexes (DRC) are to be compared. The DRCs on the left spot are symmetrical. The lower and the upper duplex are equal in length. The DRCs on the right spot have a lower duplex, which contains a single base pair mismatch. Left: the stamp is approaching the slide. Middle: the stamp is in contact with the slide. The DRCs are coupled to the streptavidin layer of the stamp via their biotinylated oligos. As the stamp is retracted, force builds up in the DRCs. Right: the stamp is removed from the slide. All DRCs are broken due to the force they have experienced. Because of the symmetrical structure of the DRCs on the left spot there is a 50–50 distribution of the Cy3-label between stamp and slide. On the right spot both DRCs are ruptured at the lower duplex, which is weaker than the upper duplex. Both Cy3-labels end up on the stamp side.

(a)

```
5' Bio-ttttttttttCTGCAGGAATTCGATATCAA   ←  biotin oligo
                 ||||||||||||||||||||
3'     Cy3-ttttt GACGTCCTTAAGCTATAGTT tttttttttttttttttt TTGATATCGAATTCCTGCAG  ←  cy3 oligo
                                                         ||||||||||||||||||||
5'                                  amino oligo  →  AACTATAGCTTAAGGACGTCttttttttttt-NH2
```

(b)

```
5'                CTGCAGGAATTCGATATCAAttttttttttt-Bio  ←  biotin oligo
                  ||||||||||||||||||||
3'     Cy3-ttttt GACGTCCTTAAGCTATAGTT tttttttttttttttttt TTGATATCGAATTCCTGCAG  ←  cy3 oligo
                                                         ||||||||||||||||||||
5'                       amino oligo  → NH2-ttttttttttt AACTATAGCTTAAGGACGTC
```

Figure 4. (a) *DRC sh-sh.* Differential rupture complex in two-fold shear geometry. Double-stranded DNA, the amino group (NH_2) for immobilization on the slide, the Cy3-fluorophore (Cy3) and the biotin residue (Bio) for the connection to the stamp are shown in bold letters. The polyT spacers are shown in regular letters. (b) *DRC zp-zp.* Differential rupture complex in two-fold zipper geometry (see (a) for details).

2.1.1. Molecules. As described above, the DRC consists of a serial assembly of three DNA oligonucleotides. A typical example is depicted in figure 4(a).

For better readability, here the DRC is drawn in horizontal orientation. Double-stranded DNA is represented by capital letters, single-stranded spacers in small letters. (The spacer sequences do not contribute to the actual base pairing. They have been introduced to separate the base pairing regions of the oligos from the slide and the stamp surface, and to allow better overall flexibility of the DRCs.) With respect to utmost symmetry, both double strands are equal in length and base composition (G–C and A–T content) and are even reverse to each other in terms of sequence. The upper oligo (to the left) is labelled with the biotin anchor, the middle oligo with the Cy3-fluorophore and the bottom oligo (right) with an amino linker for covalent immobilization. Notice that both double strands are probed in a shearing geometry, where the force builds up parallel to the double helix. A zipper geometry, where the force builds up perpendicular to the double helix, and the individual base pairs are separated in a sequential fashion, is depicted in figure 4(b).

The DRCs used in the shear–shear experiments described below, contain 30 base pair (bp) duplexes in shear mode and 60–62 nucleotides long single-stranded spacers. In completely elongated conformation, all single and double strands add up to about 60 nm in length. As estimated from a dilution series, about 10 fmol DRCs are immobilized per 1 mm^2 of the slide. This equals 10 DRCs on 100 nm $\times$ 100 nm.

It is evident that the coverage of the slide with DRCs is rather dispersed. However, a higher immobilization density of oligos might result in molecular crowding when the biotin-labelled oligos are connected to the stamp, which might interfere with the single molecule character of the experiment.

A general limitation of the differential force assay is that it has to compete with the natural (zero force) off-rate of the nucleic acid duplexes in the DRC. In case of very short DNA duplexes, low ionic strength buffers or high temperature, this natural off-rate may result in dissociation of the duplexes before the DRCs can be probed with the stamp. However, for double strands between 20 and 30 bp in 150 mM NaCl at room temperature, the spontaneous off-rates are of the order of hours to days, so these parameters are not critical.

2.1.2. Surface chemistry. A specific oriented attachment of the molecules is crucial for the outcome of the DFA, as illustrated by the shear-zip experiment described below. The altered binding geometry (5′ instead of 3′ terminus) from shear to zipper mode shifts the bond rupture force of the duplex tremendously.

For immobilization of DNA oligos on glass slides a wide variety of commercial solutions have been developed. However, the widespread ionic adsorption of the negatively charged DNA backbone to positively charged amino-functionalized surfaces cannot be used for the DFA, because this results in a rather ill-defined binding geometry of the DNA. Easily available epoxysilane slides also have limitations, because epoxy groups react with a broad range of nucleophilic residues, including intrinsic amino moieties within the nucleotides A, C and G. In our hands amino-labelled oligos attached to aldehyde slides work very well. This chemistry is reported to yield highly specific binding to the terminal amino linker. Furthermore all single-stranded spacer nucleotides are amino-free thymidines and hence do not bind to the aldehyde slide. A typical array of 16 spots on 1 cm^2 before contact with the stamp is shown in figure 6 left bottom[4].

In contrast to the commercially available slides, the surface chemistry on the silicone stamp is home-made. The silicone elastomer is activated in HCl. In experiment 2 the stamp is coated with aminosilane and grafted with reactive biotin-polyethyleneglycol (PEG) before streptavidin is bound to the surface (cf supporting online material of reference [25] for details). Alternatively, epoxysilane can be used in combination with amino-PEG-biotin. In the latter case the PEG (Rapp Polymere, Goettingen; 3000 Da) is melted at 80 °C and incubated on the stamp for 12 h, before it is washed with boiling water thoroughly (experiment 1).

2.1.3. Contact. At present, the contact area of the DFA is in the range of 1 mm^2 per spot. This could be reduced to a few μm^2 per spot, by further miniaturization. Still, the relatively large contact area is a common feature that the DFA shares with SFA. Considering the high sophistication required to bring two atomically smooth mica cylinders into contact in the SFA, it is evident that for the DFA, with multiple sample spots on each chip, a different strategy has

[4] A simple method for spotting such arrays accurately has been established just by using the same stamps as described below as a printing tool. Each pad of the stamp is loaded with a drop of the amino-modified oligo solution in upside-down orientation. Then the stamp is turned around and the pads are brought into close proximity to the slide until the drops come into contact with the surface. Due to wetting forces and gravity about 3/4 of the drop is transferred to the slide in a contact-free manner.

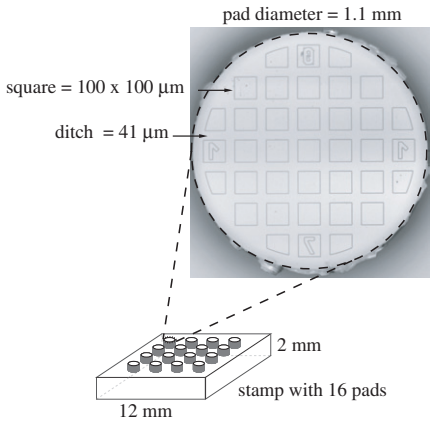

Figure 5. *Stamp structure*. A sketch of the silicone elastomer stamp is shown. The blown-up image shows the substructure of a single pad of 1.1 mm in diameter.

to be pursued to establish contact between the two surfaces. Rather than trying to perfectly level and align the two surfaces, we used one soft surface, which can conform to the other rigid surface. As soft surface, we have chosen a micro-structured silicone stamp such as is widely and successfully used for micro-contact printing, which was introduced by Whitesides [31] and co-workers. Such silicone elastomers can compensate for surface corrugations even on relatively rough surfaces, like standard microscope slides. Furthermore, they can be produced easily, by casting silicone in micro-structured moulds.

Because the stamp has to comply with the functions of uniform, conformal contact and fast drainage of buffer over an area of 1 cm^2, the geometry of the stamp is crucial for the whole experiment. The minimum requirement is a microstructure of elevated zones which come into contact with the slide, and are separated by a grid of some μm deepness. Suitable aspect ratios in terms of mechanical stability have been investigated by Delamarche *et al* for μCP [32]. The microstructures on our stamp are 100 μm $\times$ 100 μm squares with an elevation of 5 μm. The grid between the squares is about 41 μm wide, which results in a ratio of elevated to recessed surface area of approximately 1:1.[5]

As depicted in figure 5 (photograph), the microstructure is located on pads of 1.1 mm diameter and 1 mm height, which are connected to a 2 mm thick base of silicone. The 16 elevated pads shown in figure 6 (top left) are opposite to the 16 sample spots on the slide.

The pad columns increase the overall aspect ratio of the stamp and thereby improve its elastic properties. The continuous 1 mm thick stamp which was used previously in comparison has had a 8.6 times higher spring constant. The reduced contact surface, which is now restricted just to the area of the pads, and the softening in the z-direction enhance the levelling of the stamp considerably. Figure 6 (top) shows all 16 pads in contact with the slide. The image was recorded using reflection interference contrast microscopy.

[5] The moulds for the stamps are manufactured using an SOI wafer with a 5 μm thick silicon layer on top of an oxide layer. The microstructure is etched into the wafer by standard procedures. On top of the SOI wafer a Pyrex glass wafer is fixed by anodic bonding. The Pyrex wafer was structured with holes of the pad diameter, by means of ultrasonic drilling, before bonding it to the SIO wafer. Finally, the bonded SOI-Pyrex-wafer was coated with fluorosilane, in order to prevent the silicone from sticking to the mould. The bonded moulds were purchased from HSG Imit, Villingen-Schwenningen, Germany.

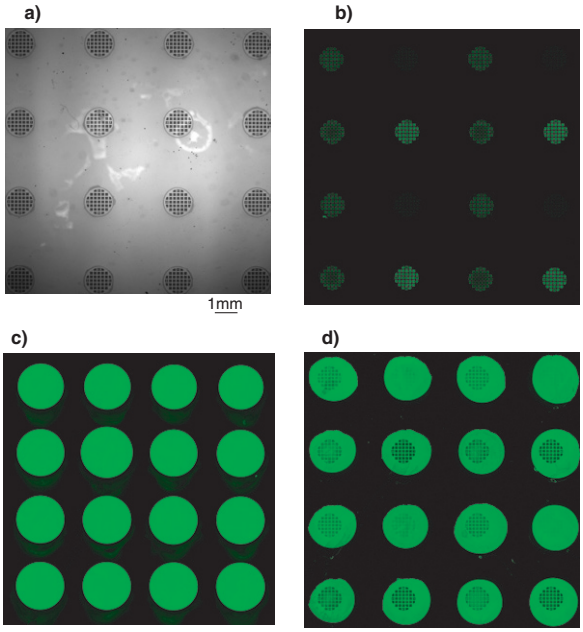

Figure 6. *Elastomer stamp and DNA-array on slide*. Reflection interference contrast micrograph of the stamp (a). Fluorescence micrographs of the stamp after contact (b), of a 16 spot DNA array on 1 cm^2 before contact (c) and of another array after contact (d).

2.1.4. Contact device. The contact device is similar to a micro-contact printing tool for soft lithography developed by the Physical Chemistry group, at the NMI Reutlingen [33]. The stamp and slide are brought into contact by means of a piezo stage (figure 7). The contact process is monitored from the bottom by reflection interference contrast microscopy (RICM). Once the gap between the silicone and the glass is of the order of the wavelength of the incident light, interference patterns are observed, until contact results in total extinction.

Figure 6 (top left) shows an RICM image of the entire stamp in contact with glass in air. In liquid, the contrast is reduced significantly, because the difference in refractive index between the stamp and the surrounding media drops from $\Delta n_{\mathrm{PDMS-air}} = 0.45$ in air to $\Delta n_{\mathrm{PDMS-water}} = 0.11$ in water. To get an overview over the whole stamp, we have used the relatively low magnification of a 1.25× objective in combination with a 16-bit CCD camera (Zeiss Axiocam). The low contrast, which is hardly resolved by eye, was enhanced by the Axiocam image processing software, using the white reference function. Adhesion of the PDMS is employed to mount the stamp onto its support.

Then stamp and slide were levelled using a tilt stage guided by the RICM image. It takes about 10 μm in z-direction from the first contact at one pad of the stamp to full contact of all pads. The corresponding contact pressure can be estimated from the Young's modulus of Sylgard184 [34] to be 17 mN mm^{-2}. If one considers that the quaternary structure of proteins remains intact up to pressures of 1 kbar, we can assume that streptavidin remains intact since we are approximately four orders of magnitude lower in pressure.

2.1.5. Coupling. As depicted in figure 3, the DRC is built up by hybridization on the slide and is subsequently connected to the streptavidin-coated stamp by means of the biotin label. The efficiency of bond formation is between 50% and 90%. Apart from several other parameters,

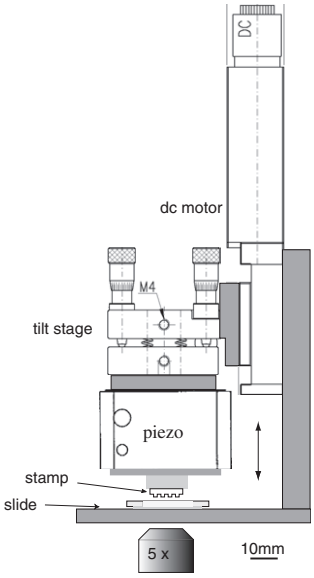

Figure 7. *Contact device*. The slide with the DNA array is located between the contact table and a trough which contains buffer solution. The stamp is mounted upside down on a glass support by adhesion. The stamp can be moved in the z-direction by the piezo stage, as well as the dc motor. Adjustment in terms of planarity between stamp and slide are accomplished by the tilt stage.

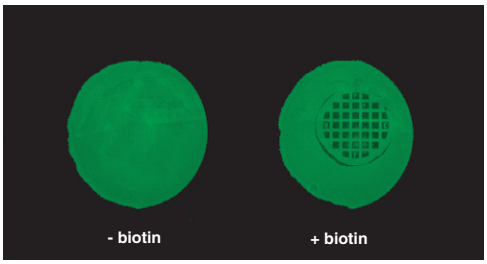

Figure 8. *Specific coupling*. Specificity of the coupling step: fluorescence micrographs of two spots on the slide after contact and removal of the stamp. The oligos on the left spot carry no biotin. The right spot is biotinylated. No Cy3–oligo was removed from the left spot, which demonstrates that the removal of Cy3–oligo from the right spot is due to specific interaction between biotin and streptavidin.

like biotin and streptavidin density and spacer length, variations in contact pressure in particular account for the broad distribution of coupling efficiencies. A sufficiently uniform contact pressure over all 16 pads hence is essential for reproducible experiments.

Once formed, the biotin–streptavidin bond is practically irreversible due to its very low off-rate. In order to demonstrate the specificity of this coupling step, the following control experiment was carried out. In figure 8 the DRC was *not* labelled with biotin on the left spot, while the right spot contained a biotinylated DRC. Consequently, on the left spot no DNA was removed from the glass slide, while on the right spot fluorescently labelled DNA was removed from the contact areas (dark squares). This demonstrates that the transfer of oligos to the stamp surface is indeed highly specific.

The coupling efficiency can be determined by labelling the free biotin residues, which have been left on the glass slide, after separation of the two surfaces, with a soluble streptavidin,

carrying a second fluorescent label. To avoid crosstalk between the two fluorescent labels, their emission and absorption spectra should be well separated. In our case we used Cy3 as a reporter within the DRC and AlexaFluor-647 as a label for the free streptavidin. Labelling with streptavidin-AF647 is done after the first scan in the Cy3-channel. Scans in the Cy3-channel are displayed in green, and scans in the AF647-channel in red (see figures 9 and 10).

2.1.6. Surface forces. Just like in AFM-based force spectroscopy, nonspecific surface interactions have to be avoided in the differential force assay. Therefore, like in AFM-based force spectroscopy, spacer molecules, here in the form of additional single strands on both ends of the DRC, are used to move the DNA duplexes away from the surfaces and separate the two surfaces from each other. Furthermore, in the set-up discussed here, attractive electrostatic forces can be neglected, because the slide, which contains carboxyl groups, and the streptavidin layer are both negatively charged at the working pH of 7.2 [7]. Also, at a NaCl concentration of 150 mM, electrostatic interactions between the surfaces are effectively screened, as the Debye length is only 0.78 nm [9] under these conditions.

However, van der Waals forces, which are not much affected by ionic strength and pH, may still contribute to the adsorption–desorption behaviour of the stamp and slide. Nevertheless, unlike in AFM and SFA experiments, in the DFA nonspecific surface to surface interactions do not interfere with the rupture forces of the individual DRCs, because the forces acting between the two chip surfaces are not measured or quantified in the experiment. Only the forces acting on the DRCs contribute to the observed results, and because the DRCs contain the sensor that actually measures the force—i.e. the reference bond in the DRC—nonspecific surface to surface forces can be ignored with this set-up.

2.1.7. Separation of stamp and slide. The pulling velocity is another important parameter for the DFA. The piezo set-up in figure 7 allows for separation velocities between nm s^{-1} and mm s^{-1}. Pulling velocities with the AFM usually do not exceed 10 μm s^{-1}, as at higher velocities deflection of the cantilever caused by hydrodynamic forces increasingly interferes with the measurement. Although hydrodynamic forces should disturb the molecular force sensors used in the DFA much less than the microscopic sensors, which are employed by other techniques, such as AFM, fluid shear stress may lead to a loss of oligonucleotides, when the silicone stamp is disrupted from the slide very rapidly. We have therefore used low pulling velocities (5 nm s^{-1} to about 1 μm s^{-1}) with the DFA so far.

As described in the introduction, the rupture force of a molecular complex with a single dissociation barrier depends logarithmically on the force loading rate. Because the slope of the f^* versus $\ln(\mathrm{d}f/\mathrm{d}t)$ curve is inversely proportional to the bond width x_b, i.e. the distance between the potential minimum and the dissociation barrier, this effect has to be considered in particular for cases where the two bonds, which are compared, have different bond widths, as is the case for DNA in shear and in zipping geometries. If the bond widths are comparable, like in the case of two 30 bp duplexes in shear geometry one containing a single mismatch and one perfect match, both bonds will be affected by the force loading rate in almost the same way. However, since the force loading rate depends not only on the pulling velocity, but also on the elasticity of the sample molecules and their molecular spacers, as well as the surface elasticity, the actual force loading rate at the DRC cannot be determined directly in our present set-up. Nevertheless, as the elasticity of the system remains constant for a certain kind of experiment, the loading rate can be assumed to be constant, as long as the pulling velocity is kept constant. The influence of the loading rate on the relative rupture probability will be discussed in more detail below.

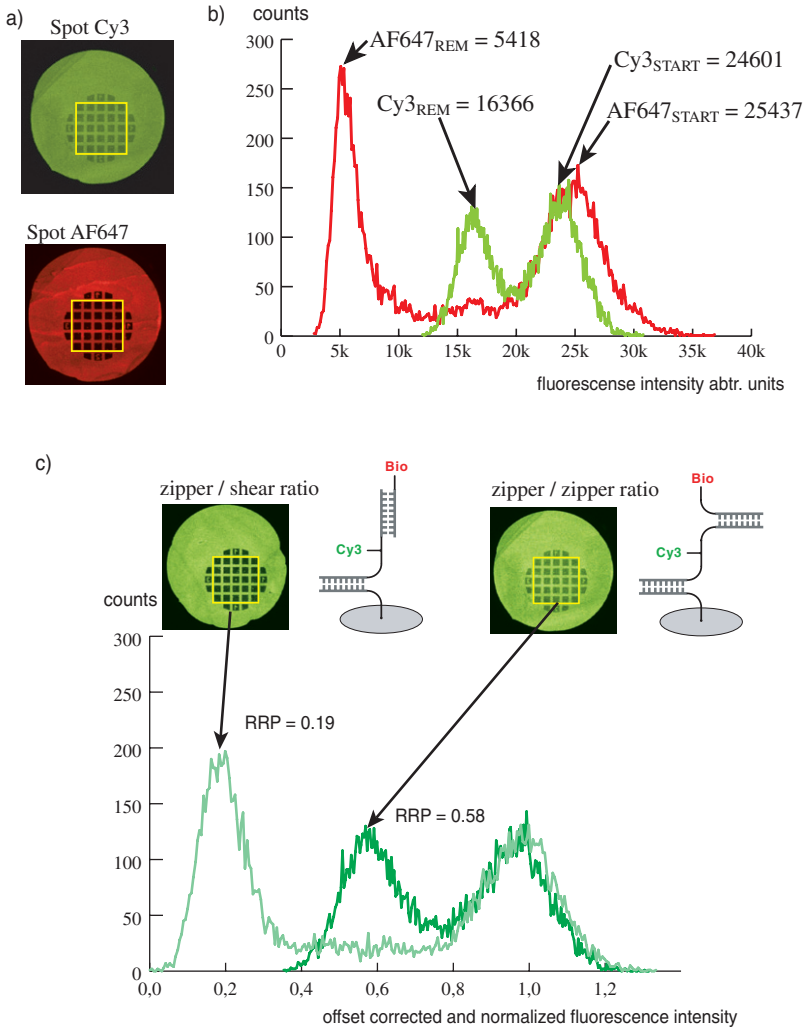

Figure 9. An experiment is presented, in which on one spot a 30 bp duplex in shear geometry is compared to a 30 bp duplex in zipper geometry and on another spot a 30 bp duplex in zipper geometry is compared to a 30 bp zipper geometry. (a) Two micrographs of the zipper/zipper spot after separation of stamp and slide are shown. The upper micrograph shows the Cy3 fluorescence intensity and the lower one the AF647 fluorescence intensity, after streptavidin labelled to AF647 was bound to the free biotins (the molecular scheme is shown in (c) on the right). (b) The histogram shows two fluorescence intensity curves corresponding to the area inside the yellow regions of interest in the spots in (a). On both curves arrows indicate the START-value for Cy3 and AF647 which corresponds to the grid in (a). The REM-values for Cy3 and AF647, corresponding to the dark squares in (a) are indicated as well. (c) The molecular structure of the shear/zipper and the zipper/zipper spots are shown schematically. The micrographs show Cy3 intensities, corrected for the offset due to molecules which did not couple, and normalized with respect to the offset corrected $Cy3_{START}$-values. The histogram again displays the regions of interest of both spots. In each curve arrows indicate the vertex of the first peak. This value corresponds to the relative rupture probability (RRP) of the lower DNA duplex. The pulling velocity of the base of the stamp was 660 nm s^{-1}.

2.1.8. Read-out. Fluorescence intensities were determined with a Tecan LS laser scanner at a spatial resolution of 6 μm. Thanks to its autofocus system, this scanner is well suited even

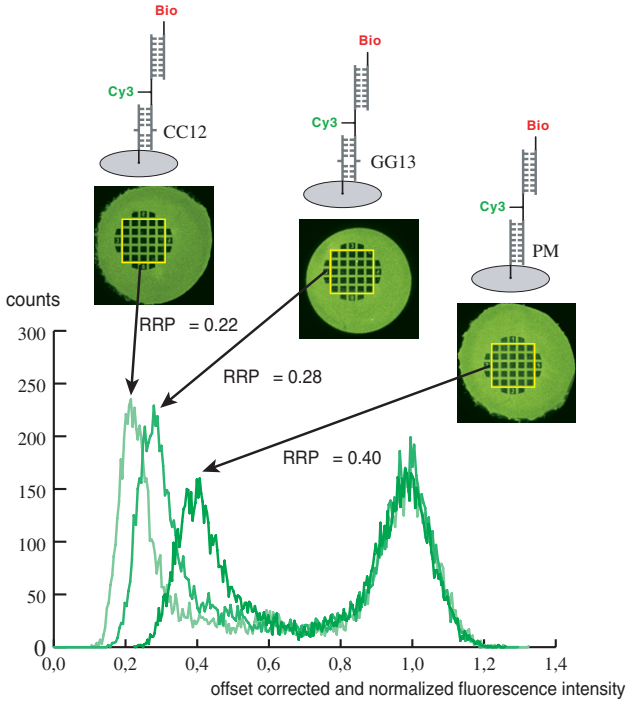

Figure 10. The molecular structures of an experiment are shown, in which the upper duplex is a 30 bp duplex in shear geometry in all three spots. The lower duplex is a 30 bp shear geometry containing a CC mismatch at position 12 on the left spot, a GG mismatch on position 13 on the middle spot and a perfect match on the right spot. The micrographs show Cy3 fluorescence intensities, corrected for the offset of non-coupled molecules and normalized to offset corrected $Cy3_{START}$-values. The histogram displays the region of interest of the three spots. In each curve arrows indicate the vertex of the first peak. This value corresponds to the relative rupture probability (RRP) of the lower DNA duplex. The pulling velocity of the base of the stamp was 5 nm s^{-1}.

for the measurement of complex surfaces, like our micro-structured silicone stamps. Cy3 was scanned at 532 nm and AF647 at 633 nm excitation wavelength.

3. Experimental results and discussion

A good example to illustrate the difference between force measurements and the measurements of reaction rate constants is depicted in figure 9. Here, two 30 bp DNA duplexes with identical sequences are compared to each other (cf figure 9(c) for a schematic drawing of the experimental set-up). In one case (left) the force is applied parallel to the helix axis, in shearing geometry; in the other case (right), the force is applied perpendicular to the helix axis, and the two strands of the double helix are separated like a zipper. In the experiment depicted in figure 9, for both geometries, the force is applied via a 30 bp DNA duplex in zipper geometry, which is attached to the slide (bottom surface) and which again contains the same base composition.

Figure 9(a) shows two fluorescence micrographs of the slide, of a typical spot where the DRCs (cf section 2.1) consist of two 30 bp DNA zippers (zip/zip). The green image (top) shows the Cy3 fluorescence intensity, after the two chip surfaces have been separated. The dark squares correspond to areas where the streptavidin-functionalized PDMS stamp has made

contact with the slide and where some of the Cy3-labelled oligos have been transferred to the stamp after the two surfaces have been separated. The fluorescence intensity of the dark squares ($Cy3_{REM}$) therefore represents DRCs, where the duplex at the bottom has remained intact after separation of the two chip surfaces. The grid pattern between the squares, on the other hand, corresponds to the micro-channels on the stamp surface. Here, as well as in the surrounding region, the stamp has not made contact with the slide, and consequently no Cy3-labelled oligos have been transferred to the stamp during the experiment. Consequently, the fluorescence intensity of the grid pattern reflects the initial DRC concentration on the slide. A histogram of fluorescence intensities (green trace in figure 9(b)) clearly shows the two corresponding peaks at fluorescence intensities of 16.4k and 24.6k.

The normalized $Cy3_{REM}$ value, i.e. the ratio of $Cy3_{REM}$ and $Cy3_{START}$, which in this case is 0.67, should therefore correlate to the relative bond rupture probability of the DNA duplex at the top of the DRC, i.e. the probability that the duplex at the top ruptures before the bottom one does. However, as already pointed out in section 2.1.5, not all of the biotin-labelled DRCs actually couple to the streptavidin-coated stamp and experience an external force, when the slide and stamp are separated. To quantify the fraction of molecules which did not couple to the stamp during the experiment, we incubated the slide with AlexaFluor-647 (AF647)-labelled streptavidin, after the slide and stamp had been separated. The red image of figure 9(a) (bottom) shows the corresponding AF647 fluorescence intensity. The remaining AF647 fluorescence intensity in the dark squares should be proportional to the number of DRCs which have not coupled to the functionalized stamp during the experiment, while the AF647 intensity on the grid should be proportional to the total number of biotin-labelled DRCs on the slide. Again, the two corresponding peaks can be clearly identified in the fluorescence intensity histogram (red trace in figure 9(c)). The ratio of AF647 intensities on squares and grid—in this case 0.21—should be equal to the fraction of DRCs which did not couple to stamp. We can use this result to correct our data and exclude those DRCs which did not couple properly to the stamp. If, for example, 21% of the DRCs did not couple to the stamp and thus did not take part in the force experiment, we simply have to subtract 21% of the $Cy3_{START}$ value from the $Cy3_{START}$ value, as well as from the $Cy3_{REM}$ value, in order count only the DRCs which actually were subjected to the external force. This subtraction is equivalent to a simple offset correction for the Cy3 fluorescence intensities. With this offset correction, the relative rupture probability (RRP) of the upper bond becomes:

$$\mathrm{RRP} = \frac{\mathrm{Cy3_{REM}} - \left(\mathrm{Cy3_{START}} \frac{\mathrm{AF647_{REM}}}{\mathrm{AF647_{START}}}\right)}{\mathrm{Cy3_{START}} - \left(\mathrm{Cy3_{START}} \frac{\mathrm{AF647_{REM}}}{\mathrm{AF647_{START}}}\right)}. \tag{3}$$

Figure 9(c) shows typical Cy3 fluorescence images both of the zip/shear and zip/zip spot, where the offset correction and the normalization—i.e. division by the offset corrected Cy3 start value—has been made directly within the image. As a consequence, in the corresponding histogram of offset corrected and normalized fluorescence intensities, the marked peak positions (left and middle), directly yield the RRP values for the two binding geometries. For the zip/shear and the zip/zip systems, the RRP values are 0.19 and 0.58 respectively.

The value of 0.58 is rather close to 50% which might be expected for a symmetrical DRC, like the one used here. However, the value of 0.19 for the shear/zip is far from 50%, although the base pairing free enthalpies, as well as the reaction rate constants of the two geometries used in this DRC, are expected to be identical. Nevertheless, when an external force is applied, the shear geometry opens more or less instantaneously, when the bond rupture force is exceeded, while in the zipper geometry the individual bases open in a consecutive manner. This corresponds to two entirely different reaction pathways in the binding potential landscape: to break a 30 bp duplex in shear geometry, a displacement of only 2 nm is required [35],

Table 1. Mean values and standard deviations of relative rupture probabilities (RRP) of a 30 bp duplex with perfectly matching sequences (GC), a GG single-base mismatch at position 13 (GG13) and a single-base mismatch at position twelve (CC12).

Duplex	RRP	σ
GC	0.41	0.013
GG13	0.28	0.004
CC12	0.21	0.014

while more than 20 nm are necessary to completely separate the two strands in the zipper geometry. According to literature values, the corresponding bond rupture forces should be around 45 and 14 pN, for shear and zipper geometry respectively [35, 19, 21, 18, 20], which is in good agreement with the low RRP of the zip/shear DRC. Nevertheless, it should be noted that, because of the statistical nature of the bond rupture process, the bond that ruptures within a DRC is not necessarily always the weaker bond in the complex. There is always a certain chance that the stronger bond, i.e. the one with the higher bond rupture force f^*, ruptures before the weaker one does, since the rupture probability distributions always have a certain overlap, where the weak bond may still be intact and the strong one may already rupture. The overlap of the two rupture probability distributions depends on the width of the distributions and on their separation, i.e. the difference $\Delta f^* = f^*_{\text{sample}} - f^*_{\text{reference}}$. Although, for a DNA zipper, the bond rupture probability distribution is rather narrow [19], the shear geometry exhibits a much broader distribution, with nonzero rupture probabilities, even at very small forces [35].

A good example of the high force resolution which can be achieved if two molecular bonds are directly compared to each other is shown in figure 10. Here, a perfectly matching 30 bp DNA duplex is compared to a 30 bp duplex with a single GG mismatch at position 13 (cf section 2.1.1 for details) and to a 30 bp duplex with a CC mismatch at position 12. Except for the indicated mismatches, all DNA duplexes again contain the same base composition. Figure 10 shows Cy3 fluorescence micrographs of typical spots for of the three DRCs, as well as the corresponding fluorescence intensity histograms. In the fluorescence images as well as in the histogram, all fluorescence intensities have been corrected for offset, and normalized with respect to the (offset-corrected) Cy3 start value, as described above for the zip/shear and zip/zip experiments. The dark green trace corresponds to the perfect match (PM), the middle one corresponds to the GG mismatch (GG13), and the light green one corresponds to the CC mismatch (CC12). The three peaks on the left-hand side of the histogram again directly reflect the RRP values of the three DRCs. The results of nine different spots (three for each DRC) are summarized in table 1. For the perfect match (GC) the mean RRP value is 0.41 ± 0.013, for the GG mismatch, it is 0.28 ± 0.004, and for the CC mismatch it is 0.21 ± 0.014. As expected, the DRC with perfect match has the highest RRP value, because the perfectly matching duplex at the bottom of the DRC is stronger than the mismatch containing duplexes of the other two DRCs, and perfect match and single nucleotide mismatch can be clearly distinguished. The value of 0.41 for the perfect match is again close to the expected 50% for a symmetric DRC.

The fact that the GG mismatch has a slightly higher RRP value than the CC mismatch is in agreement with the fact that a GG mismatch reduces the base pairing free enthalpy of DNA less than a CC mismatch, which has been attributed to the fact that although Watson–Crick base pairing is impaired for both types of mismatches, in the GG mismatch alternative hydrogen bond structures can be formed [36].

If we compare these results to AFM-based data, as indicated above, for the shear versus zip experiment, the clear discrimination of the two geometries is in good agreement with rather large Δf^* of approximately 30 pN (depending on the force loading rate), and the

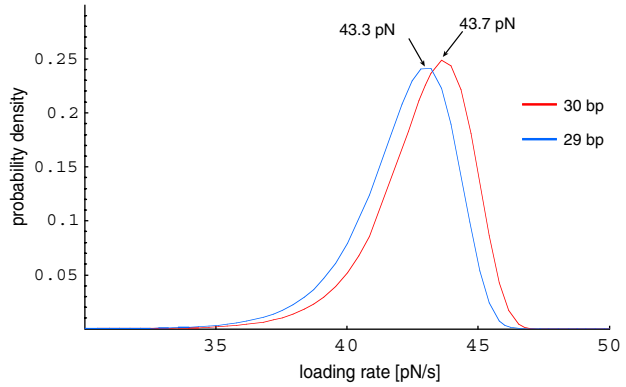

Figure 11. *Probability density functions.* Extrapolated bond rupture density probability functions for a 29 bp and a 30 bp duplex are shown. The extrapolations are based on experimental data for 10, 20, and 30 bp DNA duplexes, and on an extrapolation formula given in [35]. The blue line corresponds to the sample duplex of 29 bp, the red line to the reference complex of 30 bp. The most probable rupture forces are indicated by arrows. The force loading rate is 10^1pN s^{-1}.

narrow bond rupture probability distribution, especially of the DNA zipper. In the case of the single nucleotide mismatches, there are no direct AFM data available, because in this case the value of Δf^* is rather small and therefore extremely difficult to resolve with state of the art instrumentation. Nevertheless, one can use the interpolation formulae for $k_{\rm off}$ and for $x_{\rm b}$ given by Strunz *et al* [35], who determined the bond rupture forces of 10, 20, and 30 bp DNA duplexes by AFM, to derive bond rupture probability distributions for 29 bp and for 30 bp DNA duplexes at various force loading rates [14, 16], and use the Δf^* value as a first approximation. Figure 11 shows the calculated bond rupture probability distributions for a 29 bp and a 30 bp DNA duplex at force loading rates of 10 pN s^{-1}. This corresponds to separation velocities like those used in our experiments. The maximum (f^*) of the 29 bp distribution is at 43.3 pN, and the maximum of the 30 bp distribution is at 43.7 pN, resulting in a force difference Δf^* of only 0.4 pN. It should be pointed out, however, that this is the expected force difference if a single base is deleted at the end of one of the duplexes. In the case of a mismatch within the duplex, the nearest neighbour interactions—namely stacking interactions—with two neighbouring bases are affected, while at the end of the duplex only one nearest neighbour is actually affected. Therefore, in the case of single-base mismatch within the duplex, the expected force difference should be slightly larger than 0.4 pN. The expected force difference between a 28 bp and a 30 bp DNA duplex at 10 pN s^{-1}, which may serve an upper estimate, is 1.4 pN.

Based on our present knowledge about DNA base pairing forces, it is extremely difficult to estimate the expected force difference between a CC and a GG mismatch within a 30 bp DNA duplex. Nevertheless, our results clearly indicate that the differential force test can resolve force differences on the order of 1 pN or smaller. Yet, because a theoretical model, which would permit us to calculate the relative rupture probabilities of two bond in series, like in our DRCs, from the bond rupture probability distributions the individual bonds is still lacking, a direct comparison between AFM and DFA results is still difficult. Furthermore, in our present DFA set-up, only the separation velocity of the two surfaces can be controlled, and the force loading rate, which affects the rupture probabilities, has to be estimated from the velocity and from the elastic parameters of the stamp material. Nevertheless, although a shift in the force loading rates shifts the individual rupture probability distributions considerably, as long as the two bonds are similar, e.g. in the case of two different DNA duplexes which are both in shear

geometry, the distributions are both shifted in the same direction. Therefore, in such a case, the effect of force loading rate variations on the outcome of the experiment should be rather small.

4. Conclusion: technological applications and outlook

In this paper we have reviewed the fundamental concept, and the basic requirements, capabilities and limitations, as well as the latest technical advances, of the recently introduced differential force assay. We have discussed the conceptual difference between the measurement of rupture forces and of reaction rate constants. We have demonstrated that the differential force assay, which constitutes a completely new approach to compare intermolecular forces, has an unprecedented accuracy, as it can accurately discriminate between closely related DNA oligonucleotides, and resolve differences in bond rupture force of around 1 pN.

Although the results compare quite well with results obtained by more traditional methods, e.g. AFM-based force spectroscopy, a theoretical model for the forced dissociation of a construct containing two bonds in series, like in the DRCs, is still lacking. A suitable model would allow for direct comparison of fluorescence intensities on our chip surfaces, and bond rupture probability distributions determined from the fracture of single molecular bonds, or predict the relative rupture probabilities (RRPs) of the DRCs from single bond rupture probabilities.

As mentioned in section 1.3, a conceptually similar approach to the one discussed here has recently been described by Lang *et al* [26]. Here the external force is applied and monitored via a micro-bead in an optical trap. Their results comparing rupture forces of DNA in shear and zipper geometry agree quite well our data. The fact that the force which is applied to the DRC can be directly monitored and quantified with the optical trap is an evident advantage of the set-up used by Lang *et al*. With this set-up, it is not only possible to discriminate between different bond rupture forces, but the bond rupture force of the weaker bond, as well as the force loading rate, can be accurately determined. On the other hand, our approach uses a standard biochip format. This opens the door for technological applications of the DFA, which go far beyond comparing bond rupture forces of biomolecular bonds. The compatibility with standard biochip formats [25, 37, 38] allows for the use of the DFA for highly parallel diagnostic applications in a simple and straightforward manner. Because the DFA compares bond rupture forces, rather than equilibrium binding constants, like conventional biochips, it has the potential to overcome some of the shortcomings and limitation conventional DNA and protein biochip formats. Because in the DFA the two chip surfaces are separated on a millisecond to second timescale (the whole process takes a few seconds), slow thermal dissociation does not slow down the assay. Consequently, time-consuming washing steps, like overnight stringency washing, can be avoided. This is extremely valuable, especially for the analysis and detection of high-affinity binders, which play an increasingly important role in drug development and diagnostics, and which may have thermal off-rates of the order of days. In particular, when it comes to comparing large libraries of high-affinity binders and selecting the desired molecules—something which is traditionally done with surface plasmon spectroscopy—the DFA may speed up the selection process significantly. Furthermore, by choosing appropriate force references for each spot on a chip, it should in principle be possible to achieve stringent binding conditions for analyte molecules with different binding constants. And it has already been shown that the specificity and also the sensitivity, both extremely critical assay parameters of multiplexed sandwich immuno-assays (i.e. protein biochips), can be drastically improved [30].

Acknowledgments

The authors would like to acknowledge Gregor Neuert for providing the probability density simulations, E Sackmann for helpful discussions, and D Braun, M Stelzle and Philip Severin for support regarding the design of the contact device and the silicon moulds. This work was supported by the Deutsche Forschungsgemeinschaft (DFG).

References

[1] Bensimon D 1996 *Structure* **4** 885
[2] Merkel R 2001 *Phys. Rep.-Rev. Section of Phys. Lett.* **346** 344
[3] Janshoff A, Neitzert M, Oberdorfer Y and Fuchs H 2000 *Angew. Chem.-Int. Edn* **39** 3213
[4] Rief M and Grubmuller H 2002 *Chem. Phys. Chem.* **3** 255
[5] Clausen-Schaumann H, Seitz M, Krautbauer R and Gaub H E 2000 *Curr. Opin. Chem. Biol.* **4** 524
[6] Israelachvili J N and Tabor D 1972 *Proc. R. Soc.* A **331** 19
[7] Leckband D 2000 *Annu. Rev. Biophys. Biomol. Struct.* **29** 1
[8] Israelachvili J and Wennerstrom H 1996 *Nature* **379** 219
[9] Israelachvili J N 1992 *Intermolecular and Surface Forces* (San Diego, CA: Academic)
[10] Urbakh M, Klafter J, Gourdon D and Israelachvili J 2004 *Nature* **430** 525
[11] Beyer M K and Clausen-Schaumann H 2005 *Chem. Rev.* **105** 2921
[12] Zhurkov S N 1965 *Int. J. Fract. Mech.* **1** 311
[13] Bell G I 1978 *Science* **200** 618
[14] Evans E and Ritchie K 1997 *Biophys. J.* **72** 1541
[15] Evans E and Ritchie K 1999 *Biophys. J.* **76** 2439
[16] Evans E 2001 *Annu. Rev. Biophys. Biomol. Struct.* **30** 105
[17] Merkel R, Nassoy P, Leung A, Ritchie K and Evans E 1999 *Nature* **397** 50
[18] Essevaz-Roulet B, Bockelmann U and Heslot F 1997 *Proc. Natl Acad. Sci. USA* **94** 11935
[19] Bockelmann U, Essevaz-Roulet B and Heslot F 1997 *Phys. Rev. Lett.* **79** 4489
[20] Rief M, Clausen-Schaumann H and Gaub H E 1999 *Nat. Struct. Biol.* **6** 346
[21] Bockelmann U 2004 *Curr. Opin. Struct. Biol.* **14** 368
[22] Clausen-Schaumann H, Rief M, Tolksdorf C and Gaub H E 2000 *Biophys. J.* **78** 1997
[23] Gittes F and Schmidt C F 1998 *Eur. Biophys. J. Biophys. Lett.* **27** 75
[24] Viani M B, Schaffer T E, Chand A, Rief M, Gaub H E and Hansma P K 1999 *J. Appl. Phys.* **86** 2258
[25] Albrecht C, Blank K, Lalic-Multhaler M, Hirler S, Mai T, Gilbert I, Schiffmann S, Bayer T, Clausen-Schaumann H and Gaub H E 2003 *Science* **301** 367
[26] Lang M J, Fordyce P M, Engh A M, Neuman K C and Block S M 2004 *Nat. Methods* **1** 133
[27] Ekins R P and Chu F 1994 *Trends Biotechnol.* **12** 89
[28] Lipschutz R J, Fodor S P A, Gingeras T R and Lockhart D J 1999 *Nat. Genet.* **21** 20
[29] Mitchell P 2002 *Nat. Biotechnol.* **20** 225
[30] Blank K, Lankenau A, Mai T, Schiffmann S, Gilbert I, Hirler S, Albrecht C, Benoit M, Gaub H E and Clausen-Schaumann H 2004 *Anal. Bioanal. Chem.* **379** 974
[31] Xia Y and Whitesides G M 1998 *Annu. Rev. Mater. Sci.* **28** 153
[32] Delamarche M and Biebuyck H 1997 *Adv. Mater.* **9** 741
[33] http://www.nmi.de/englisch/showprj.php3?id=65&bereich=3&typ=2
[34] Engel J C J M, Bullen D and Liu C 2004 mass.micro.uiuc.edu/publications/papers/133.pdf
[35] Strunz T, Oroszlan K, Schafer R and Guntherodt H J 1999 *Proc. Natl Acad. Sci. USA* **96** 11277
[36] Hyther 2006 http://ozone2.chem.wayne.edu/Hyther/hythermenu.html
[37] Blank K, Mai T, Gilbert I, Schiffmann S, Rankl J, Zivin R, Tackney C, Nicolaus T, Spinnler K, Oesterhelt F, Benoit M, Clausen-Schaumann H and Gaub H E 2003 *Proc. Natl Acad. Sci. USA* **100** 11356
[38] Gilbert L, Schiffmann S, Rubenwolf S, Jensen K, Mail T, Albrecht C, Lankenau A, Beste G, Blank K, Gaub H E and Clausen-Schaumann H 2004 *Proteomics* **4** 1417